

Simple, Efficient, and Generic Post-Selection Decoding for qLDPC codes

Haipeng Xie,¹ Nobuyuki Yoshioka,² Kento Tsubouchi,³ and Ying Li^{1,*}

¹Graduate School of China Academy of Engineering Physics, Beijing 100193, China

²International Center for Elementary Particle Physics, University of Tokyo, 7-3-1 Hongo, Bunkyo-ku, Tokyo 113-0033, Japan

³Department of Applied Physics, University of Tokyo, 7-3-1 Hongo, Bunkyo-ku, Tokyo 113-8656, Japan

Quantum error correction is indispensable for scalable quantum computation. Although encoding logical qubits substantially enhances noise resilience, achieving logical error rates low enough for practical algorithms remains challenging on existing hardware. Here we introduce argument reweighting, a simple and broadly applicable post-selection decoding strategy that boosts the performance of maximum-likelihood-type decoders, including minimum-weight perfect matching and belief-propagation families. The method suppresses logical errors by performing additional decoding rounds under reweighted error models, enabling acceptance of high-confidence syndrome outcomes. Circuit-level simulations across multiple decoders and qLDPC codes show that argument reweighting substantially suppresses logical errors, requiring a rejection rate of only 1.44×10^{-5} to reduce the logical error rate by almost two orders of magnitude for the $[[144, 12, 12]]$ bivariate bicycle code. These results establish argument reweighting as a practical and resource-efficient approach for enhancing quantum fault tolerance.

I. INTRODUCTION

Quantum error correction is essential for enabling many promising applications of quantum computation, such as large-integer factorization and high-accuracy simulation of quantum many-body systems [1–5]. A central challenge in realizing quantum error correction is the substantial qubit overhead: increasing the code distance to achieve a target logical fidelity requires more physical qubits [6, 7]. Recent efforts have focused on developing low-overhead quantum error correction techniques, particularly high-rate quantum low-density parity-check (qLDPC) codes [8–10]. Alongside code design, improving decoding performance is equally important, as a more effective decoder can suppress logical errors without additional qubit resources [11–14].

Incorporating post-selection into the decoding process offers a practical means to further reduce logical errors. By using measured error syndromes and derived information, one can accept or reject a circuit run, designing the acceptance rule to trade a finite rejection rate for lower logical error rates; see Fig. 1(a). While simple acceptance rules, such as rejecting runs based on detector density or correction weight, can significantly suppress logical errors, they typically incur a high rejection rate [15–18]. More sophisticated rules have been explored, including boundary-edge modification for minimum-weight perfect matching (MWPM) decoders, referred to as complementary gap [19–22], and error-sparsity estimation via cluster analysis for clustering-based decoders, referred to as error-cluster statistics [18]. Nevertheless, a post-selection strategy that is both efficient and broadly compatible across different decoders and codes has yet to be established.

In this work, we introduce *argument reweighting*, a simple and generic post-selection decoding scheme. Its gen-

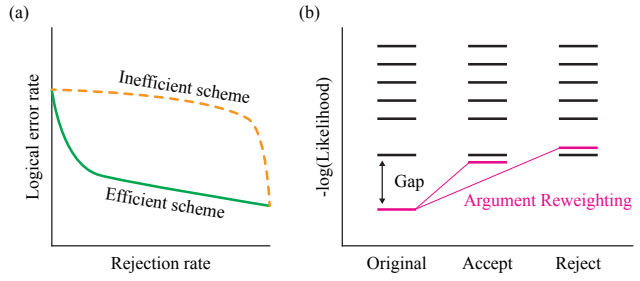


FIG. 1. (a) Efficiency of post-selection decoding. A post-selection scheme trades a rejection rate for a reduction in the logical error rate. The scheme is deemed more efficient if it achieves the same logical-error suppression at a smaller rejection rate. (b) Schematic illustration of argument reweighting (shown with the physical-error criterion). In a maximum-likelihood-type decoder, the correction corresponds to the most likely error configuration among all those compatible with the measured syndrome, which are represented by horizontal bars. The first decoding round uses the original error model and outputs the candidate correction (highlighted in magenta). In the second round, the error model is modified to suppress the likelihood of this candidate, and decoding is performed again. The circuit run is accepted if and only if the second-round output agrees with the first; otherwise, it is rejected.

erality stems from its compatibility with any maximum-likelihood-type decoder—those that determine corrections by exactly or approximately maximizing a likelihood (or related objective) derived from an error model. This class encompasses most widely used decoders, including MWPM and belief propagation (BP) [23–27]; see Table I. Furthermore, argument reweighting is universally applicable across diverse quantum codes. The scheme is also remarkably simple, requiring only minor modifications to the underlying decoder. We employ a multi-round decoding process, accepting a circuit run only if all rounds yield the same (or equivalent) cor-

* yli@gscap.ac.cn

rection. In each subsequent round, the decoder's error model is reweighted based on the previous output [see Fig. 1(b)].

Numerical simulations demonstrate that argument reweighting efficiently suppresses logical errors. We apply the method to a range of decoders, including MWPM and three variants of BP, and test it on rotated surface codes [28] as well as instances from the bivariate bicycle (BB) code family [10]. We observe a clear trend that the method becomes increasingly efficient with growing code distance: at larger distances, the logical error rate decreases more rapidly as the rejection rate increases. For the BP-OSD decoder applied to the $[[144, 12, 12]]$ BB code [10], argument reweighting reduces the logical error rate from 9.08×10^{-7} to 1.41×10^{-8} at a rejection rate of only 1.44×10^{-5} after 12 rounds of parity-check measurements. We further compare our method with existing post-selection strategies for qLDPC codes, including detector density, correction weight, and error-cluster statistics, and find that argument reweighting outperforms them, achieving up to a two-order-of-magnitude reduction in logical error rate at substantially lower rejection rates. Moreover, all of the above results are obtained within circuit-level noise models, and we further show that the scheme operates seamlessly with sliding-window decoding frameworks [23, 29–31], underscoring its direct relevance to practical fault-tolerant quantum computation.

Decoder	App.	Decoder	App.
MWPM [23, 24]	✓	BP-OSD [26, 27]	✓
Union Find [32, 33]	○	BP-LSD [34]	✓
BP [25]	○	BP-AC [35]	○
Mem-BP [36]	○	Tesseract [37]	○
BP-GD [31, 38]	○	DTDs [39]	○
Relay-BP [13]	✓	Neural Network [12]	✗

TABLE I. Applicability of argument reweighting across various quantum error correction decoders. Our scheme is supported for decoders labeled with a check mark (benchmarked in this work) or a circle (supported in principle but not yet benchmarked). Decoders marked with a cross are incompatible.

II. ARGUMENT REWEIGHTING

We first introduce our method in the context of maximum-likelihood decoding and then apply it to two representative practical decoders: MWPM and BP-type (such as BP-OSD and Relay-BP).

Maximum likelihood decoding. Let e denote a physical Pauli error. A stabilizer quantum error correction code defines a mapping from e to the measured syndrome in parity-check measurements, denoted by $S(e)$, and a mapping from e to the corresponding logical error, denoted by $L(e)$.

In maximum-likelihood decoding [40], the correction is

determined from a physical error model M , which specifies the probability of each error e , denoted $\Pr(e; M)$. Given an observed syndrome s , the decoder outputs the correction

$$c \in \arg \max_{e: S(e)=s} \Pr(e; M), \quad (1)$$

meaning that c is chosen from arguments of the maximum likelihood.

In argument reweighting, a second round of decoding is performed using a modified error model M' , in which the likelihood of the first-round correction c is suppressed in one of two ways [see Fig. 1(b)]:

$$\text{Gap test: } \Pr(c; M') = e^{-b} \Pr(c; M), \quad (2)$$

$$\text{Ratio test: } \Pr(c; M') = [\Pr(c; M)]^b, \quad (3)$$

where b is a tunable parameter that controls the strength of the suppression, with $b > 0$ for gap test and $b > 1$ for ratio test. Ideally, the probabilities of all other errors sharing the same syndrome are kept unchanged. We emphasize that this condition need not be enforced strictly in practical implementations. Under the modified model, maximum-likelihood decoding produces a second correction

$$c' \in \arg \max_{e: S(e)=s} \Pr(e; M'). \quad (4)$$

The circuit run is accepted according to the criterion:

- *Physical-error criterion (PEC)*—Accept iff $c' = c$.

We now explain why our approach reduces the logical error rate. The total logical error rate can be expressed as the average of the logical error rates conditioned on the observed syndrome s . The goal of post-selection is to reject those circuit runs whose syndrome s is associated with a high conditional logical error rate. Importantly, the conditional logical error rate is upper bounded by the conditional probability of the complement of c given s , i.e., the probability that the true error configuration does not correspond to the decoder's output. Furthermore, this conditional complementary probability can be upper bounded in terms of the log-likelihood gap between the most probable error configuration and the next most probable one; see Fig. 1(b) and Appendix A. A large log-likelihood gap implies high confidence that the conditional logical error rate is small. Gap test, together with PEC, is designed to detect such gaps and thereby identify high-confidence syndromes for acceptance. We note that complementary gap decoding [19–22], a post-selection scheme for surface codes, operates on a similar principle: it probes the likelihood gap by modifying boundary edges of the decoding graph.

In our framework, ratio test serves an analogous purpose to gap test: both compare the most and next most probable error configurations, but ratio test does so through the ratio of their log-likelihoods. Equivalently, ratio test may be viewed as a variant of gap test with an adaptive gap criterion. Specifically, Eq. (2) can be

recovered from Eq. (3) by replacing the fixed suppression factor e^{-b} with the adaptive factor $[\Pr(c; M)]^{b-1}$. We emphasize that in practice neither gap test nor ratio test provides an accurate detection of the true likelihood gap (because probabilities of errors other than c are usually also changed); nevertheless, numerical results show that both mechanisms are effective, with ratio test slightly outperforms gap test (see Appendix B).

In addition to the physical-error criterion, we find that certain variants can further improve performance. Since all corrections within the same logical equivalence class produce the same logical effect, we may relax the acceptance condition to

- *Two-round logical-error criterion (2R-LEC)*—Accept iff $L(c') = L(c)$.

We may also strengthen the confidence of acceptance by performing a third round of decoding, using a reweighted error model M'' that suppresses the likelihoods of both c and c' . Let c'' be the output of the third-round decoding under M'' . This leads to an enhanced rule:

- *Three-round logical-error criterion (3R-LEC)*—Accept iff $L(c'') = L(c') = L(c)$.

Note that one can further increase the number of reweighting-decoding rounds.

MWPM. The decoding is performed on a weighted graph (V, E, w) , where V is the set of nodes representing parity checks, E is the set of edges corresponding to elementary errors, and $w : E \rightarrow \mathbb{R}$ assigns a weight to each edge. Under the error model, an elementary error $q \in E$ occurs with probability $p(q)$. The edge weights are defined as $w(q) = \ln[1/p(q) - 1]$, effectively mapping error probabilities to additive weights [23]. A physical error configuration e is represented by a subset of edges $e \subseteq E$, and an observed syndrome s corresponds to a subset of nodes $s \subseteq V$. MWPM aims to find a set of paths that pair up all nodes in s while minimizing the total weight, which is equivalent to maximizing the likelihood. The union of the edges on these paths constitutes the correction $c \subseteq E$.

In argument reweighting, based on the first-round output c , we modify the error model by adjusting the elementary error probabilities. For the ratio test variant, the modified probabilities are defined as

$$p'(q) = \begin{cases} p(q)^b, & q \in c, \\ p(q), & q \notin c, \end{cases} \quad (5)$$

where $b > 1$ is the suppression parameter. When a second reweighting round is performed, the updated probabilities p'' are derived analogously by modifying p' based on the second-round output c' . See Appendix B for the gap test version.

BP. The decoding is performed on a Tanner (bipartite) graph (C, B, E) , where C is the set of nodes corresponding to parity checks, B is the set of nodes representing

elementary errors, and $E \subseteq C \times B$ specifies which elementary errors are detected by which checks. As in MWPM decoding, an elementary error $q \in B$ occurs with probability $p(q)$; a physical error configuration is a subset $e \subseteq B$; and a measured syndrome is a subset $s \subseteq C$. Given s , BP iteratively exchanges messages between C and B , updating marginal likelihoods until convergence (or until a maximum number of iterations is reached). A final decision is then made, yielding a correction $c \subseteq B$.

In argument reweighting, we modify the error model in the same manner as in MWPM, using Eq. (5), with the only difference that the correction c is now a subset of B . Pseudocodes for MWPM and BP decoding corresponding to the three acceptance criteria are provided in Appendix C.

III. NUMERICAL PERFORMANCE AND BENCHMARKS

We evaluate the performance of PEC and LEC on both rotated surface codes and BB codes using their respective mainstream decoders. Simulations are performed under a standard circuit-level noise model with physical error rate $p = 0.1\%$; see Appendix D for details. As shown in Figs. 2(a) and (b), under PEC, the logical error rates of both rotated surface codes and BB codes decrease steadily as the rejection rate increases, for both MWPM and BP-OSD decoders. As a more permissive strategy, LEC substantially improves post-selection efficiency in the low-rejection-rate regime, which is the most relevant in practice. However, under LEC, the logical error rate reduction eventually saturates: beyond a certain rejection rate, additional post-selection yields no further improvement. This saturation threshold can be pushed by increasing the number of reweighting-decoding rounds. Consistent with the data, 3R-LEC achieves lower logical error rates than 2R-LEC, albeit at the cost of increased runtime; see Appendix E for an explanation. We note that employing additional reweighting-decoding rounds can yield even further reductions in the logical error rate; numerical results for the 4R-LEC scheme are provided in Appendix B.

Figs. 2(c)-(f) illustrate the performance of 3R-LEC across a range of decoders, including MWPM, BP-OSD, BP-LSD, and Relay-BP, evaluated on additional code examples. We observe that 3R-LEC becomes increasingly efficient with growing code distance: at larger distances, the logical error rate decreases more rapidly as the rejection rate increases; see Appendix B for plots of rescaled logical error rates, which illustrate the post-selection efficiency more transparently. Furthermore, 3R-LEC consistently achieves a one-order-of-magnitude suppression of logical errors across all tested decoders and code instances, and reaches two orders of magnitude for codes with sufficiently large distances. For the BP-OSD (Relay-BP) decoder applied to the $[[144, 12, 12]]$ BB code, argument reweighting reduces the logical error rate from

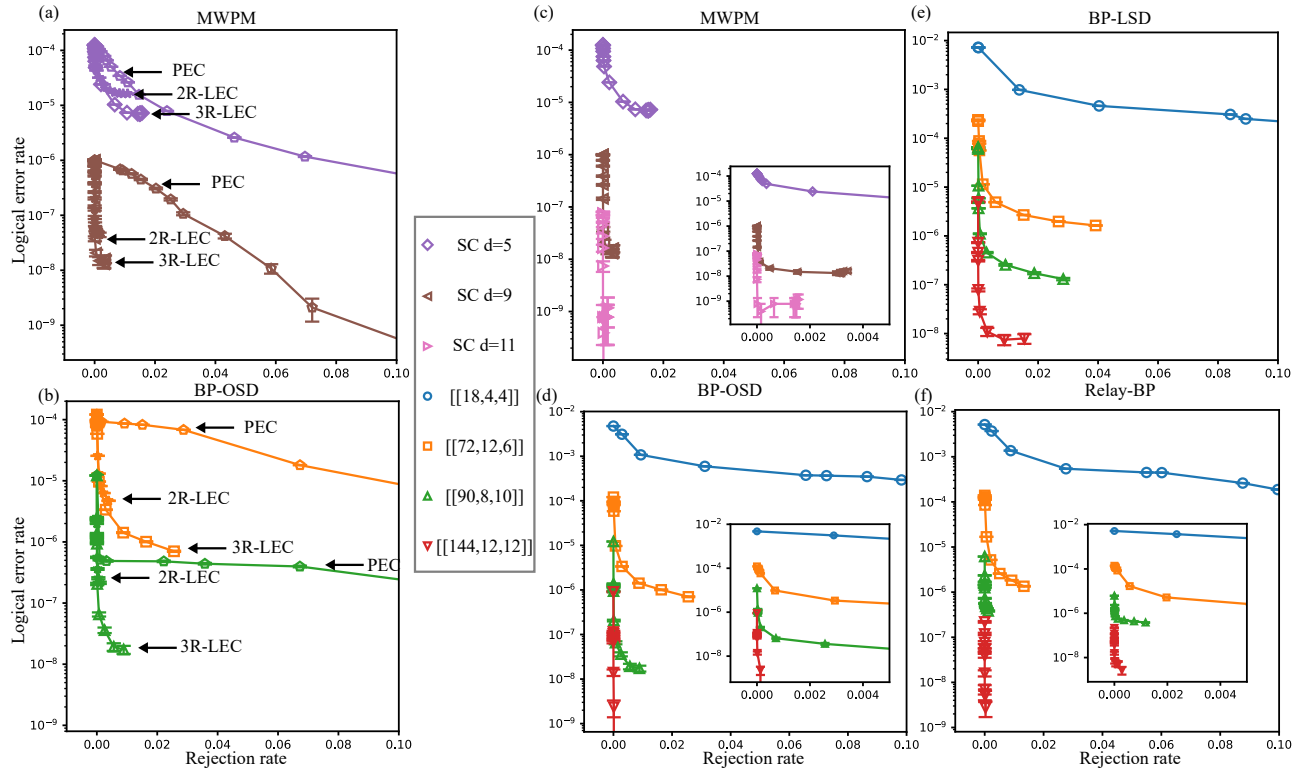


FIG. 2. Total logical error rate after d rounds of parity-check measurements, where d denotes the code distance. We simulated rotated surface codes ($d = 5, 9, 11$) [28] and four BB code instances ($[[18, 4, 4]]$, $[[72, 12, 6]]$, $[[90, 8, 10]]$, and $[[144, 12, 12]]$) [10, 41]. Results are obtained using the ratio test variant defined in Eq.(5). Further details regarding the simulation are provided in Appendix D.

9.08×10^{-7} (2.20×10^{-7}) to 1.41×10^{-8} (1.60×10^{-8}) at a rejection rate of only 1.44×10^{-5} (1.83×10^{-6}) after 12 rounds of parity-check measurements.

IV. COMPARISONS WITH OTHER POST-SELECTION STRATEGIES

A key advantage of our post-selection strategy over complementary gap [19–22] and error-cluster statistics [18] is its broad applicability across decoders, rather than being limited to a specific family.

In terms of efficiency, when applied to BB codes, 3R-LEC significantly outperforms error-cluster statistics, achieving a one- to two-order-of-magnitude suppression of logical errors at substantially lower rejection rates (Fig. 3). We note that this comparison is performed using the BP-LSD decoder, while our 3R-LEC scheme is also compatible with other decoders for qLDPC codes. Complementary gap is currently inapplicable to general qLDPC codes. For surface codes, complementary gap achieves higher efficiency (see Appendix B), as it estimates the likelihood gap more accurately via decoding-graph modifications.

Regarding runtime, our method requires only a small, fixed number of decoding rounds (at most three in prac-

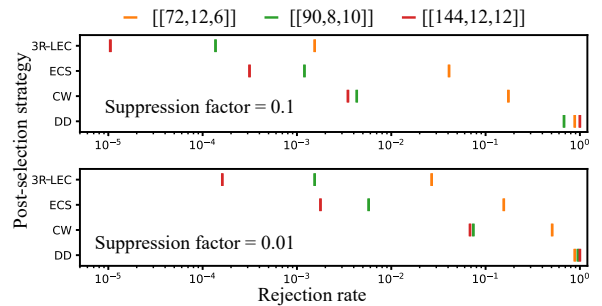


FIG. 3. Efficiency of various post-selection strategies applied to the BP-LSD decoder. The performance of four strategies—3R-LEC, error-cluster statistics (ECS), correction weight (CW), and detector density (DD) [18]—is compared across three BB code instances. For each code, we estimate the rejection rates (per d parity-check cycles) required to reduce the logical error rate by one and two orders of magnitude. We find that our method (3R-LEC) consistently requires the lowest rejection rate among all post-selection strategies considered. We note that the rejection rates for 3R-LEC are reported as conservative upper bounds, whereas those for other strategies are calculated precisely (subject to statistical error); see Appendix D for further details.

tice, as shown in our numerical results), incurring a

moderate computational overhead. In comparison, while error-cluster statistics operates with a single decoding round, the runtime of complementary gap scales exponentially with the number of logical qubits k . Specifically, complementary gap requires 2^k rounds to evaluate all logical equivalence classes, rendering it impractical for multi-logical-qubit scenarios. Such cases include high-rate code blocks encoding multiple logical qubits [8–10], as well as the collective decoding of transversal controlled-NOT gate sequences or lattice surgery operations involving multiple surface-code blocks [42, 43]. In contrast, our strategy maintains a small number of decoding rounds, remaining computationally tractable even for the 12-logical-qubit cases examined in our numerical results.

V. SCALABLE APPLICATION IN FAULT-TOLERANT QUANTUM COMPUTATION

The applicability of post-selection is limited by the rejection rate. Let r denote the rejection rate per logical gate. A circuit with N logical gates succeeds with probability $(1 - r)^N \simeq e^{-Nr}$, implying $N \lesssim 1/r$ to maintain a reasonable overall success. Nevertheless, post-selection decoding can still be applied to large-scale fault-tolerant quantum computation through two approaches. First, it is well suited for small resource-state preparation and distillation circuits, such as those for magic states [44–47]. For large-scale circuits, the computation can be decomposed into smaller subcircuits implemented via gate teleportation [9, 48–51], with post-selection applied to preparation circuits of gate-teleportation resource states. Repeating each preparation independently allows the overall failure probability to be efficiently suppressed. Second, post-selection can be used for error mitigation on logical qubits. In the spacetime noise inversion approach, “super qubits”—logical qubits with error rates much lower than standard logical qubits—are required for error sampling, avoiding the complexity of characterizing the full error model [52]. Because these sampling circuits are small and independent, post-selection can be applied to them efficiently to realize super qubits. The accuracy of the error-mitigated computation is then determined by the logical error rate of these super qubits, and post-selection effectively suppresses the computational bias to the level set by the logical error rate achieved under post-selection decoding.

VI. APPLICATION TO SLIDING WINDOW DECODING

Sliding window decoding [23, 29–31] is an important approach for real-time decoding, which is essential for the practical deployment of quantum error correction in quantum computation. In this scheme, syndrome data are decoded over successive finite time intervals, referred

to as windows. Each window consists of $n_{\text{com}} + n_{\text{buf}}$ rounds of parity-check measurements and is divided into two parts: the first n_{com} rounds form the commit region, while the remaining n_{buf} rounds constitute the buffer region. The decoding algorithm is applied to the entire window, but the resulting correction is effectively committed only to the commit region; errors in the buffer region are deferred and corrected in the subsequent windows.

Argument reweighting seamlessly extends to sliding window decoding. For each window, we reweight the error model across the entire window based on the correction from the previous decoding round of the same window. Post-selection is then performed using our proposed acceptance criteria. Numerical results for this sliding window implementation are provided in Appendix B, demonstrating that argument reweighting in sliding window decoding yields performance comparable to that in global decoding. Furthermore, we evaluated a variant where reweighting is restricted solely to the commit region; however, we find that reweighting the entire window provides superior results.

VII. HIGH-REJECTION-RATE LIMIT

We now analyze the performance of reweighting in the high-rejection-rate limit, focusing on the variant defined in Eq. (5). In the limit $b \rightarrow +\infty$, the likelihood of any non-empty correction c vanishes. Consequently, a non-empty c is never produced as the output of the second decoding round, i.e., $c \neq c'$. According to PEC, a circuit run is always rejected if $c \neq c'$. Therefore, in this limit, PEC only accepts runs where c is empty, i.e. no syndrome is observed; effectively, this doubles the code distance, representing the maximum possible suppression of the logical error rate [22].

This argument does not apply directly to LEC, as runs with non-empty c can still pass post-selection even as $b \rightarrow +\infty$; see Appendix E for further details. Our numerical results indicate that the limiting logical error rate for LEC decreases as the number of reweighting-decoding rounds increases. However, whether the LEC logical error rate asymptotically approaches the doubled-distance limit of PEC remains a subject for further investigation.

VIII. CONCLUSIONS

In this work, we introduced argument reweighting, a post-selection decoding strategy applicable to a broad class of decoders and quantum error correction codes. We benchmarked its performance using circuit-level simulations across multiple decoders and codes, and demonstrated compatibility with sliding window decoding. Among the three rejection criteria we propose, 3R-LEC offers the best trade-off between logical error suppression and rejection rate in the low-rejection regime. Our

numerical results show that the method typically yields two to three orders of magnitude reduction in logical error rate, with a significantly smaller rejection rate than existing post-selection approaches. These results establish argument reweighting as a practical and efficient tool for enhancing logical reliability, particularly in early fault-tolerant quantum computing architectures where resource efficiency is critical.

ACKNOWLEDGMENTS

This work is supported by the National Natural Science Foundation of China (Grant Nos. 12225507, 12088101) and NSAF (Grant No. U1930403). N.Y. is supported by JST Grant Number JPMJPF2221, JST CREST Grant Number JPMJCR23I4, IBM Quantum, JST ASPIRE Grant Number JPMJAP2316, JST ERATO Grant Number JPMJER2302, and Institute of AI and Beyond of the University of Tokyo. The source codes for the numerical simulation are available at [53].

Appendix A: Bounds on the conditional logical error rate

The probability of observing syndrome s is

$$\Pr(s) = \sum_{e : S(e)=s} \Pr(e; M). \quad (\text{A1})$$

For the raw maximum-likelihood decoding, the logical error probability conditioned on s is

$$p_L(s) = 1 - \frac{\sum_{e : S(e)=s, L(e)=L(c)} \Pr(e; M)}{\Pr(s)}, \quad (\text{A2})$$

where c is the correction produced by the decoder with the input syndrome s . This probability is upper bounded by

$$p_L(s) \leq 1 - \frac{\Pr(c; M)}{\Pr(s)}. \quad (\text{A3})$$

The total logical error probability without post-selection is

$$p_{L,\text{tot}} = \sum_s \Pr(s) p_L(s). \quad (\text{A4})$$

Let e_{next} denote the next most probable error, i.e.,

$$e_{\text{next}} \in \arg \max_{e : S(e)=s, e \neq c} \Pr(e; M), \quad (\text{A5})$$

and define the likelihood gap Δ by

$$\Pr(e_{\text{next}}; M) = e^{-\Delta} \Pr(c; M). \quad (\text{A6})$$

Let $m = |\{e : S(e) = s\}|$ be the total number of errors with syndrome s . Then

$$\frac{\Pr(c; M)}{\Pr(s)} \geq \frac{\Pr(c; M)}{\Pr(c; M) + (m-1)\Pr(e_{\text{next}}; M)} = \frac{1}{1 + (m-1)e^{-\Delta}}, \quad (\text{A7})$$

and consequently

$$p_L(s) \leq 1 - \frac{1}{1 + (m-1)e^{-\Delta}} < (m-1)e^{-\Delta}. \quad (\text{A8})$$

Appendix B: Additional numerical results

1. More reweighting-decoding rounds

While we focused on 2R-LEC and 3R-LEC in the main text, this reweighting-decoding procedure generalizes naturally to additional rounds. For example, by constructing a modified error model M''' that suppresses the likelihoods of the preceding corrections $\{c, c', c''\}$, one can obtain a fourth-round output c''' . This defines the following enhanced decision rule:

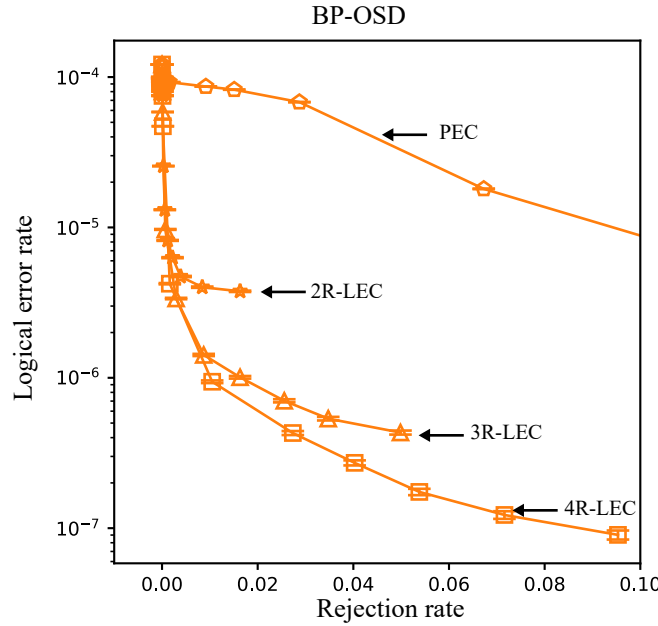


FIG. 4. Performance with increasing reweighting-decoding rounds. Results are shown for the $[[72,12,6]]$ BB code using the BP-OSD decoder.

- *Four-round logical-error criterion (4R-LEC)*—Accept iff $L(c''') = L(c'') = L(c') = L(c)$.

The performance of this 4R-LEC scheme is illustrated in Fig. 4. As shown, 4R-LEC further improves post-selection efficiency and pushes the saturation threshold, albeit at the cost of increased runtime.

2. Logical error suppression factor

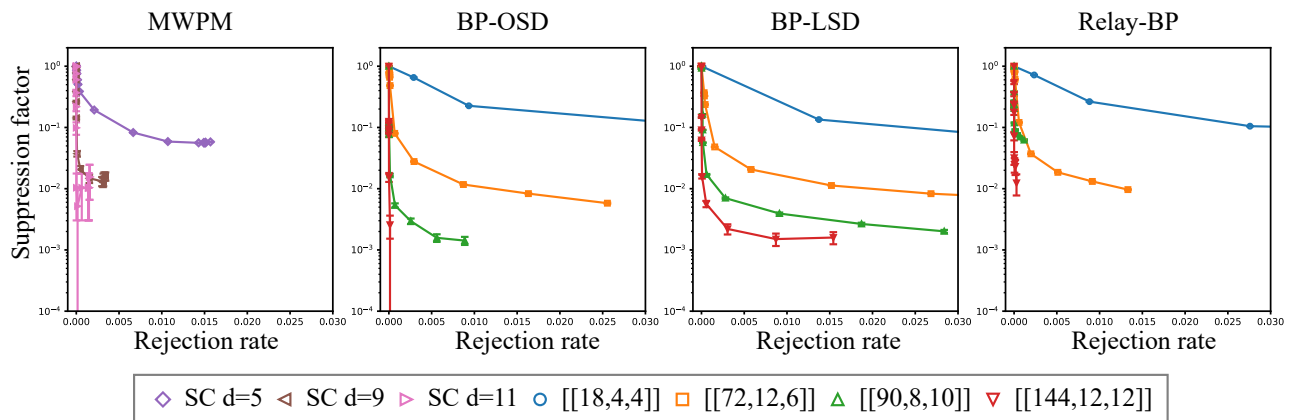


FIG. 5. Logical error suppression factor. For each decoder and code, the suppression factor is defined as the logical error rate at a given rejection rate divided by the logical error rate without post-selection.

In Figs. 2(c)–(f) of the main text, we illustrate the relationship between the logical error rate and the rejection rate

of 3R-LEC across various codes and decoders. To better evaluate the performance of 3R-LEC, Fig. 5 presents these results in a normalized form, where the logical error rates are expressed relative to the baseline error rates without post-selection.

3. Gap test

For the gap test version, with the error configuration c from the first-round decoding, we modify the error model by taking

$$p'(q) = \begin{cases} \exp\left(-\frac{\ln p(q)}{\ln p(c)}b\right)p(q), & q \in c, \\ p(q), & q \notin c, \end{cases} \quad (\text{B1})$$

where $p(c) = \prod_{q \in c} p(q)$, and $b > 0$ is the suppression parameter.

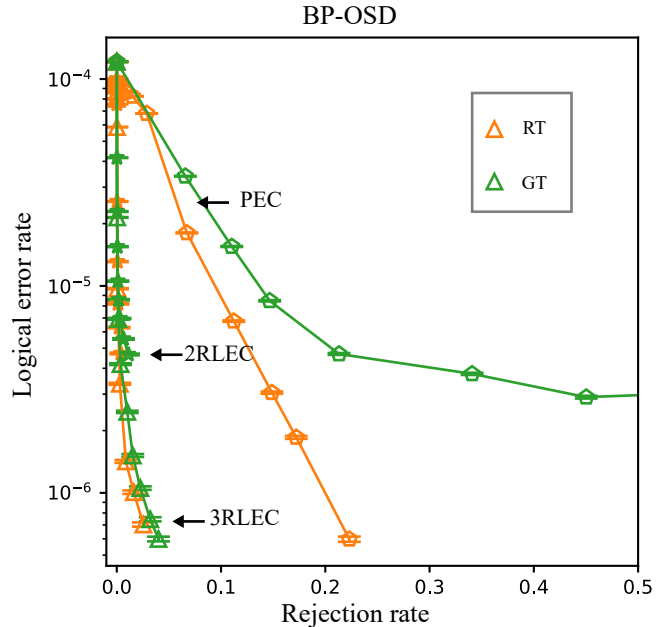


FIG. 6. Comparison between the ratio test (RT) and gap test (GT). Performance is evaluated for the [[72,12,6]] BB code using the BP-OSD decoder.

The performance of the gap test is shown in Fig. 6. Following the definition in Eq.(B1), we consider eight distinct values of the reweighting parameter: $b \in \{2, 5, 7, 10, 12, 15, 20, 25\}$. Our results indicate that the ratio test slightly outperforms the gap test in terms of post-selection efficiency.

4. Comparison with the complementary gap method

To compare 3R-LEC with the complementary gap method, we evaluate both strategies on a distance $d = 9$ rotated surface code using the MWPM decoder. As illustrated in Fig. 7, 3R-LEC and the complementary gap method exhibit comparable efficiency in the low-rejection-rate regime. However, as the rejection rate increases, the complementary gap method begins to outperform 3R-LEC.

We have further performed numerical analysis to understand the difference between two methods, as shown in Fig. 8. As the value of complementary gap increases, the conditional logical error rate drops exponentially, which allows efficient rejection scheme. When we employ the 3R-LEC, we find that erroneous shots with small complementary gaps are also accepted. This provides a numerical support for our discussion in Appendix E that performance of LEC is currently limited by the shielding effect.

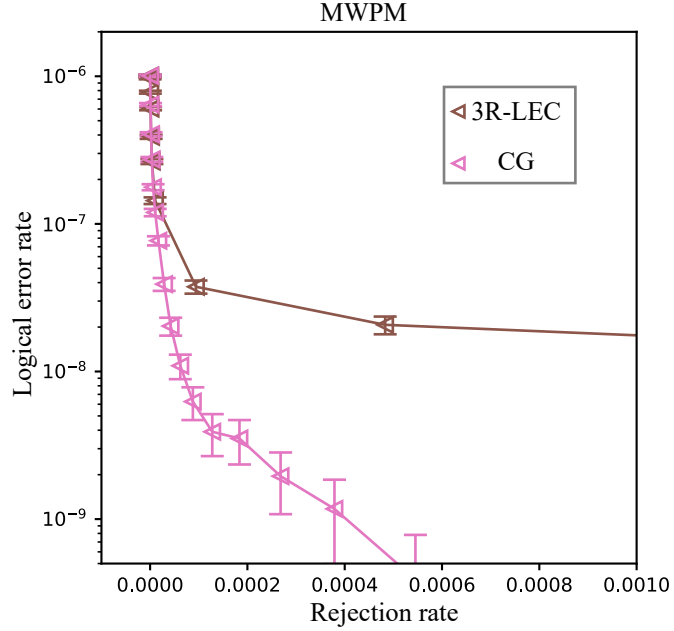


FIG. 7. Comparison between 3R-LEC and the complementary gap (CG) method. Results are shown for the $d = 9$ rotated surface code after d rounds of parity-check measurements, decoded using the MWPM decoder.

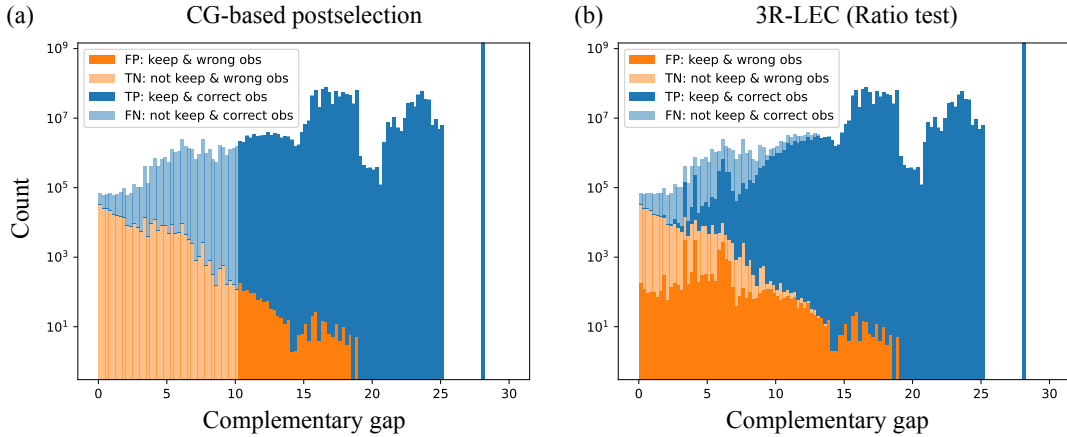


FIG. 8. Histogram of success/failure by postselection. The blue and orange colors indicate whether the prediction by decoder is correct or not, and thick/faint colors discriminate whether the shot was kept or not. Here, we consider $d = 5$ rotated surface code using the MWPM decoder for d rounds of syndrome extraction. (a) postselection based on complementary gap method with the threshold value taken as 10. (b) 3R-LEC using ratio test with reweighting parameter $b = 2.5$. The rejection rates are 0.012 and 0.014, respectively.

5. Integration with sliding-window decoding

In sliding-window decoding, each window comprises a commit region and a buffer region, allowing our method to be applied flexibly to different regions. We evaluate two specific strategies: applying 3R-LEC to the decoded elementary errors across the entire window, or restricting the reweighting to those within the commit region. As illustrated in Fig. 9, both approaches are effective, with the former being more efficient and achieving performance nearly identical to that of 3R-LEC under global decoding.

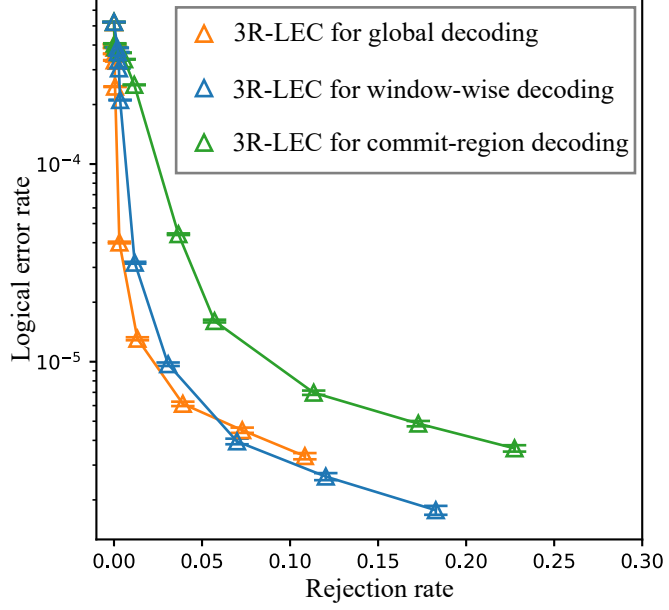


FIG. 9. Performance of 3R-LEC under global and sliding-window decoding. Results show the total logical error rate of the $[[72, 12, 6]]$ BB code after $4d$ rounds of parity-check measurements using the BP-OSD decoder, where d is the code distance. For sliding-window decoding, each $2d$ -round window is partitioned into a d -round commit region and a d -round buffer region.

Appendix C: Pseudocodes

The algorithms in this section utilize the following notation:

- $\text{DECODER}(p, s) \rightarrow c$: A maximum-likelihood-type decoder that accepts an error model p and a syndrome s as input. Here, $p : E \rightarrow \mathbb{R}$ specifies the prior probabilities for the set of elementary errors E , and c is the resulting physical correction.
- Logical Map L : A function that maps a physical error (or correction) to its corresponding logical error class.
- Post-Selection Strategy R : The specific scheme employed, where $R \in \{\text{PEC}, \text{2R-LEC}, \text{3R-LEC}\}$.
- Reweighting Parameter b : The tunable parameter used in the modified error models to control the strength of suppression during subsequent decoding rounds.

Algorithm 1 Post-Selection Decoding via Argument Reweighting

```

1: function ARGUMENTREWEIGHTING(DECODER,  $p$ ,  $s$ ,  $L$ ,  $R$ ,  $b$ )
2:    $c \leftarrow \text{DECODER}(p, s)$                                       $\triangleright$  Obtain first-round correction based on priors  $p$  and syndrome  $s$ 
3:   if  $c = \emptyset$  then                                          $\triangleright$  If no error is detected, the run is accepted by default
4:     return Accept,  $c$ 
5:   Flag  $\leftarrow \text{POSTSELECTION}(\text{DECODER}, p, s, L, R, b, c)$ 
6:   if Flag = 1 then
7:     return Accept,  $c$ 
8:   else
9:     return Reject

```

Algorithm 2 Post-Selection

```

1: function POSTSELECTION(DECODER,  $p$ ,  $s$ ,  $L$ ,  $R$ ,  $b$ ,  $c$ )
2:   Flag  $\leftarrow 0$ 
3:    $p' \leftarrow \text{REWEIGHTING}(p, b, c)$                                  $\triangleright$  Generate first modified error model
4:    $c' \leftarrow \text{DECODER}(p', s)$                                       $\triangleright$  Second round of decoding
5:   if  $R = \text{PEC}$  then                                             $\triangleright$  Physical-Error Criterion
6:     if  $c' = c$  then
7:       Flag  $\leftarrow 1$ 
8:     else if  $R = 2\text{R-LEC}$  then                                          $\triangleright$  Two-Round Logical-Error Criterion
9:       if  $L(c') = L(c)$  then
10:      Flag  $\leftarrow 1$ 
11:    else if  $R = 3\text{R-LEC}$  then                                          $\triangleright$  Three-Round Logical-Error Criterion
12:      if  $L(c') = L(c)$  then
13:         $p'' \leftarrow \text{REWEIGHTING}(p', b, c')$                                  $\triangleright$  Generate second modified error model
14:         $c'' \leftarrow \text{DECODER}(p'', s)$                                       $\triangleright$  Third round of decoding
15:        if  $L(c'') = L(c)$  then
16:          Flag  $\leftarrow 1$ 
17: return Flag

```

Algorithm 3 Reweighting—Eq. (5)

```

1: function REWEIGHTING( $p, b, c$ )
2:    $p' \leftarrow p$                                                $\triangleright$  Initialize the modified error model
3:   for each elementary error  $q \in c$  do
4:      $p'(q) \leftarrow p(q)^b$                                           $\triangleright$  Suppress the likelihood of the previous correction
5:   return  $p'$ 

```

Appendix D: Details of numerical simulations**1. Circuits and noise model**

Simulations are performed using rotated surface-code circuits based on the *Stim* library [54] and BB code circuits from Ref. [31]. We assume a circuit-level noise model with a physical error rate of $p = 0.001$, characterized by the following:

- Single-qubit Clifford gates are subject to depolarizing noise with probability p , where each Pauli error X , Y , or Z occurs with probability $p/3$.
- Two-qubit Clifford gates are subject to two-qubit depolarizing noise with probability p ; each of the 15 non-trivial two-qubit Pauli errors occurs with probability $p/15$.
- Idling qubits undergo depolarizing noise with probability p during each time step.
- State preparation and resets in the Z (X) basis are followed by a bit-flip X (phase-flip Z) error with probability p .
- Measurement outcomes are flipped with probability p .

All syndrome sampling and circuit simulations are conducted using the *Stim* library.

2. Decoder implementation

We utilize several open-source libraries for our decoder implementations: MWPM is implemented via *PyMatching* [24], BP-OSD and BP-LSD are sourced from the *ldpc* library [27], and the Relay-BP decoder is implemented using the *relay* library [13]. We employ optimized parameter configurations for each decoder to ensure a high-performance comparison.

For MWPM, we utilize the default settings [24].

For BP-OSD, we take the following parameters [31]:

- `max_iter`: 200
- `bp_method`: “minimum_sum”
- `ms_scaling_factor`: 1.0
- `osd_method`: “OSD_CS”
- `osd_order`: 10

For BP-LSD, we take the following parameters [18, 34]:

- `max_iter`: 30
- `bp_method`: “minimum_sum”
- `ms_scaling_factor`: 1.0
- `lsd_method`: “LSD_0”
- `lsd_order`: 0

For Relay-BP, we take the following parameters [13, 55, 56]:

- `gamma0`: 0.125
- `pre_iter`: 80
- `num_sets`: 300
- `set_max_iter`: 60
- `gamma_dist_interval`: (-0.24, 0.66)
- `stop_nconv`: 1

3. Post-Selection parameters and sample sizes

By varying the control parameter $b = 1 + z$, we obtain post-selected logical error rates across a range of rejection rates. For the surface code results shown in Fig. 2, we employ a consistent set of 17 values for z : $\{10^{-12}, 10^{-6}, 10^{-3}, 0.01, 0.02, 0.04, 0.06, 0.1, 0.2, 0.3, 0.4, 0.5, 0.6, 0.7, 0.8, 0.9, 1\}$. For the BB codes, 10 distinct values of z are used. Specifically, we set $z \in \{10^{-8}, 0.1, 0.5, 1, 1.5, 2, 2.5, 3, 3.5, 4\}$ for the $[[18, 4, 4]]$ code, and $z \in \{10^{-15}, 10^{-8}, 10^{-4}, 10^{-3}, 0.01, 0.1, 0.2, 0.3, 0.4, 0.5\}$ for the remaining BB codes. For any given code, the parameter b remains identical across all tested decoders.

To ensure high statistical precision, we sampled 2.56×10^9 instances for each code-decoder pair. For each value of b , the post-selected logical error rate and its standard deviation are estimated from the retained instances. We note that higher values of b lead to increased rejection rates, thereby reducing the effective sample size of the retained data.

4. Comparison between post-selection strategies

To evaluate the efficiency of different post-selection strategies, we define two primary metrics: (1) the rejection rate required to achieve a tenfold reduction (one order of magnitude) in the logical error rate, and (2) the rejection rate required for a hundredfold reduction (two orders of magnitude). Strategies that achieve these targets at lower rejection rates are considered more efficient.

We determine the rejection rates corresponding to tenfold ($\eta = 0.1$) and hundredfold ($\eta = 0.01$) reductions in the logical error rate as follows. First, we evaluate the baseline logical error rate p_L and its standard deviation σ_L without post-selection. For a given post-selection configuration, let p'_L and σ'_L denote the resulting logical error rate and its associated standard deviation, respectively. We define the target ηp_L as being “achieved” if the two rates are within one standard deviation, i.e.,

$$|\eta p_L - p'_L| \leq \sqrt{(\eta \sigma_L)^2 + \sigma'^2_L}. \quad (\text{D1})$$

η	Code	Baseline	3R-LEC	ECS	CW	DD
10^{-1}	[[72,12,6]]	0 $2.379(3) \times 10^{-4}$	$1.5435(8) \times 10^{-3}$ $1.145(7) \times 10^{-5}$	$4.0964(4) \times 10^{-2}$ $2.38(1) \times 10^{-5}$	$1.74331(7) \times 10^{-1}$ $2.31(2) \times 10^{-5}$	$8.83231(6) \times 10^{-1}$ 0
	[[90,8,10]]	0 $6.49(2) \times 10^{-5}$	$1.370(2) \times 10^{-4}$ $5.91(5) \times 10^{-6}$	$1.2003(7) \times 10^{-3}$ $6.49(5) \times 10^{-6}$	$4.312(1) \times 10^{-3}$ $6.5(8) \times 10^{-6}$	$6.78411(9) \times 10^{-1}$ $6.11(6) \times 10^{-6}$
	[[144,12,12]]	0 $4.98(4) \times 10^{-6}$	$1.051(6) \times 10^{-5}$ $4.6(1) \times 10^{-7}$	$3.142(4) \times 10^{-4}$ $5.0(1) \times 10^{-7}$	$3.473(1) \times 10^{-3}$ $5(2) \times 10^{-7}$	$9.999159(2) \times 10^{-1}$ 0
	[[72,12,6]]	0 $2.379(3) \times 10^{-4}$	$2.6838(3) \times 10^{-2}$ $1.97(3) \times 10^{-6}$	$1.56154(7) \times 10^{-1}$ $2.38(3) \times 10^{-6}$	$5.07449(10) \times 10^{-1}$ $1.29(10) \times 10^{-7}$	$8.83231(6) \times 10^{-1}$ 0
	[[90,8,10]]	0 $6.49(2) \times 10^{-5}$	$1.5426(8) \times 10^{-3}$ $6.6(2) \times 10^{-7}$	$5.762(1) \times 10^{-3}$ $6.5(2) \times 10^{-7}$	$7.4081(5) \times 10^{-2}$ $6.4(6) \times 10^{-7}$	$9.52405(4) \times 10^{-1}$ $5.4(1) \times 10^{-7}$
	[[144,12,12]]	0 $4.98(4) \times 10^{-6}$	$1.614(3) \times 10^{-4}$ $4.6(4) \times 10^{-8}$	$1.7750(8) \times 10^{-3}$ $5.0(4) \times 10^{-8}$	$6.8386(5) \times 10^{-2}$ $5(2) \times 10^{-8}$	$9.999159(2) \times 10^{-1}$ 0

TABLE II. Numerical results for the BP-LSD decoder using the 3R-LEC, error-cluster statistics (ECS), correction weight (CW), and detector density (DD) methods. For each code, the upper (lower) row reports the corresponding rejection rate (logical error rate). See the text for an explanation regarding the zero observed logical error rates for the DD method.

The target is considered “surpassed” if p'_L is significantly lower than the target, satisfying the condition:

$$\eta p_L - p'_L > \sqrt{(\eta \sigma_L)^2 + \sigma'_L^2}. \quad (\text{D2})$$

For the 3R-LEC scheme, the post-selection process is controlled by the parameter b . Because evaluating each value of b requires a complete execution of the decoding algorithm, an exhaustive search for a configuration that exactly achieves the target is time consuming. Consequently, we terminate the parameter search once we identify a configuration that achieves or surpasses the target while remaining close to it.

In contrast, for the other three strategies—error-cluster statistics (ECS), correction weight (CW), and detector density (DD)—adjusting the post-selection threshold does not require additional decoding rounds. This allows us to precisely identify a configuration that achieves the target logical error rate for ECS and CW. The case of DD is unique: here, the rejection rate is controlled by a threshold on the syndrome weight (the number of triggered detectors). In our simulations, we frequently encountered scenarios where the target logical error rate could not be met at any finite threshold, and the only remaining option is a stringent acceptance rule that rejects all instances with a non-zero syndrome weight. Such a rule results in extremely low logical error rates, yielding zero observed logical errors within our finite sample size. Therefore, for DD, we report the configuration that achieves the target rate when possible; otherwise, we report the results of the zero-weight acceptance rule. The resulting data are presented in Table II.

In Table II, the baseline, 3R-LEC, CW, and DD are evaluated based on the raw BP-LSD decoder provided by the *ldpc* library, while ECS is evaluated using the *ldpc-post-selection* library, which was developed in Ref. [18] to implement the BP-LSD decoder with the ECS approach. We find that a discrepancy exists between the logical error rates of the standard *ldpc* library and those of the *ldpc-post-selection* library, even when the latter is operated without post-selection. Specifically, the *ldpc-post-selection* implementation yields logical error rates that are higher by a factor of about two across the three code instances, suggesting potential room for improvement.

Appendix E: Explanation of the saturation phenomenon in LEC

The set of all physical errors can be partitioned into equivalence classes according to their corresponding logical effects. Ideally, decoding is performed by evaluating the total likelihood of each class and selecting the most probable one. In practice, however, decoders typically identify the single most likely physical error (the correction) rather than the most likely class; this can be viewed as approximating the total likelihood of a class by the likelihood of the most probable physical error in the class. When the likelihood gap between the most-likely and next-most-likely classes is small, the correction is more prone to resulting in a logical error. Therefore, the goal of post-selection is to reject instances characterized by a narrow gap between these two leading classes.

Argument reweighting probes this likelihood gap by modifying the error model. A plausible explanation for the observed saturation phenomenon is a *shielding effect*: high-likelihood physical errors belonging to the same logical class as the initial correction can effectively “shield” errors in competing classes. Consequently, these alternative classes remain undetected during the reweighting process, even when the true gap is small.

This mechanism can be understood through the spectrum of negative log-likelihoods illustrated in Fig. 10. As an example, consider a spectrum containing two logical classes, represented by solid and dashed lines, respectively. The

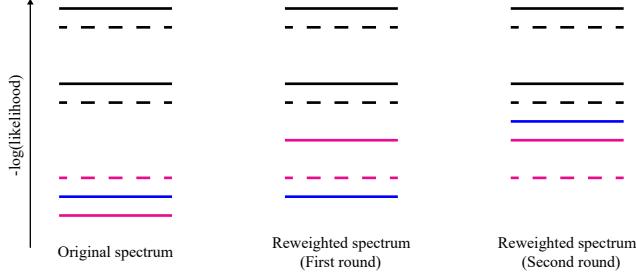


FIG. 10. Negative log-likelihood spectrum of physical errors.

most likely physical error (the red solid line) belongs to the “solid” class and is selected as the correction. Suppose that the next most likely physical error (the blue solid line) also belongs to the solid class, while the third most likely error (the red dashed line) belongs to the “dashed” class. If the red dashed line is close to the red solid line, the instance should ideally be rejected due to the small gap.

In the PEC scheme, reweighting lifts the red solid line (making it less likely). The decoder then selects the next most likely error, which is the blue solid line. Since the physical correction has changed, PEC correctly rejects the instance, though it does so based on the gap between physical errors rather than the gap between classes.

However, in 2R-LEC, the instance is accepted because the new most likely error (blue solid) still belongs to the same class as the original correction. Despite the narrow gap between the two classes (the proximity of the red dashed line to the red solid line), the instance remains accepted because the dashed class was shielded by the blue solid line. Due to this shielding effect, an instance may be accepted regardless of how high the red solid line is lifted. This explains the behavior in the large- b limit, where the performance of the post-selection scheme saturates.

This picture also illustrates the improvement offered by 3R-LEC. In the second round of reweighting, the blue solid line is also lifted. This finally allows the red dashed line from the alternative class to become the most likely correction. Consequently, 3R-LEC detects the competing class and rejects the instance.

Finally, we note that argument reweighting, as implemented in practice [e.g., in Eq. (5)], modifies the likelihood of all elementary errors within a correction. This collective modification of the error model may also contribute to the saturation phenomenon in addition to the shielding effect described above.

[1] A. R. Calderbank and P. W. Shor, Good quantum error-correcting codes exist, *Phys. Rev. A* **54**, 1098 (1996).

[2] A. G. Fowler, M. Mariantoni, J. M. Martinis, and A. N. Cleland, Surface codes: Towards practical large-scale quantum computation, *Phys. Rev. A* **86**, 032324 (2012).

[3] E. Knill, R. Laflamme, and W. H. Zurek, Resilient quantum computation, *Science* **279**, 342 (1998).

[4] C. Gidney, How to factor 2048 bit RSA integers with less than a million noisy qubits (2025), [arXiv:2505.15917](https://arxiv.org/abs/2505.15917).

[5] R. Babbush, C. Gidney, D. W. Berry, N. Wiebe, J. McClean, A. Paler, A. Fowler, and H. Neven, Encoding Electronic Spectra in Quantum Circuits with Linear T Complexity, *Phys. Rev. X* **8**, 041015 (2018).

[6] D. Aharonov and M. Ben-Or, Fault-Tolerant Quantum Computation With Constant Error Rate (1999), [arXiv:quant-ph/9906129](https://arxiv.org/abs/quant-ph/9906129).

[7] Google Quantum AI and Collaborators, R. Acharya, D. A. Abanin, L. Aghababaie-Beni, I. Aleiner, T. I. Andersen, M. Ansmann, F. Arute, K. Arya, A. Asfaw, N. Astrakhantsev, J. Atalaya, R. Babbush, D. Bacon, B. Ballard, J. C. Bardin, J. Bausch, A. Bengtsson, A. Bilmes, S. Blackwell, S. Boixo, G. Bortoli, A. Bourassa, J. Bovaard, L. Brill, M. Broughton, D. A. Browne, B. Buchea, B. B. Buckley, D. A. Buell, T. Burger, B. Burkett, N. Bushnell, A. Cabrera, J. Campero, H.-S. Chang, Y. Chen, Z. Chen, B. Chiaro, D. Chik, C. Chou, J. Claes, A. Y. Cleland, J. Coogan, R. Collins, P. Conner, W. Courtney, A. L. Crook, B. Curtin, S. Das, A. Davies, L. De Lorenzo, D. M. Debro, S. Demura, M. Devoret, A. Di Paolo, P. Donohoe, I. Drozdov, A. Dunsworth, C. Earle, T. Edlich, A. Eickbusch, A. M. Elbag, M. Elzouka, C. Erickson, L. Faoro, E. Farhi, V. S. Ferreira, L. F. Burgos, E. Forati, A. G. Fowler, B. Foxen, S. Ganjam, G. Garcia, R. Gasca, E. Genois, W. Giang, C. Gidney, D. Gilboa, R. Gosula, A. G. Dau, D. Graumann, A. Greene, J. A. Gross, S. Habegger, J. Hall, M. C. Hamilton, M. Hansen, M. P. Harrigan, S. D. Harrington, F. J. H. Heras, S. Heslin, P. Heu, O. Higgott, G. Hill, J. Hilton, G. Holland, S. Hong, H.-Y. Huang, A. Huff, W. J. Huggins, L. B. Ioffe, S. V. Isakov, J. Iveland, E. Jeffrey, Z. Jiang, C. Jones, S. Jordan,

C. Joshi, P. Juhas, D. Kafri, H. Kang, A. H. Karamlou, K. Kechedzhi, J. Kelly, T. Khaire, T. Khattar, M. Khezri, S. Kim, P. V. Klimov, A. R. Klots, B. Kobrin, P. Kohli, A. N. Korotkov, F. Kostritsa, R. Kothari, B. Kozlovskii, J. M. Kreikebaum, V. D. Kurilovich, N. Lacroix, D. Landhuis, T. Lange-Dei, B. W. Langley, P. Laptev, K.-M. Lau, L. Le Guevel, J. Ledford, J. Lee, K. Lee, Y. D. Lensky, S. Leon, B. J. Lester, W. Y. Li, Y. Li, A. T. Lill, W. Liu, W. P. Livingston, A. Locharla, E. Lucero, D. Lundahl, A. Lunt, S. Madhuk, F. D. Malone, A. Maloney, S. Mandrà, J. Manyika, L. S. Martin, O. Martin, S. Martin, C. Maxfield, J. R. McClean, M. McEwen, S. Meeks, A. Megrant, X. Mi, K. C. Miao, A. Mieszala, R. Molavi, S. Molina, S. Montazeri, A. Morvan, R. Movassagh, W. Mruczkiewicz, O. Naaman, M. Neeley, C. Neill, A. Nersisyan, H. Neven, M. Newman, J. H. Ng, A. Nguyen, M. Nguyen, C.-H. Ni, M. Y. Niu, T. E. O'Brien, W. D. Oliver, A. Opremcak, K. Ottosson, A. Petukhov, A. Pizzuto, J. Platt, R. Potter, O. Pritchard, L. P. Pryadko, C. Quintana, G. Ramachandran, M. J. Reagor, J. Redding, D. M. Rhodes, G. Roberts, E. Rosenberg, E. Rosenfeld, P. Roushan, N. C. Rubin, N. Saei, D. Sank, K. Sankaragomathi, K. J. Satzinger, H. F. Schurkus, C. Schuster, A. W. Senior, M. J. Shearn, A. Shorter, N. Shutty, V. Shvarts, S. Singh, V. Sivak, J. Skruzny, S. Small, V. Smelyanskiy, W. C. Smith, R. D. Somma, S. Springer, G. Sterling, D. Strain, J. Suchard, A. Szasz, A. Sztein, D. Thor, A. Torres, M. M. Torunbalci, A. Vaishnav, J. Vargas, S. Vdovichev, G. Vidal, B. Villalonga, C. V. Heidweiller, S. Waltman, S. X. Wang, B. Ware, K. Weber, T. Weidel, T. White, K. Wong, B. W. K. Woo, C. Xing, Z. J. Yao, P. Yeh, B. Ying, J. Yoo, N. Yosri, G. Young, A. Zalcman, Y. Zhang, N. Zhu, and N. Zobrist, Quantum error correction below the surface code threshold, *Nature* **638**, 920 (2025).

[8] N. P. Breuckmann and J. N. Eberhardt, Quantum Low-Density Parity-Check Codes, *PRX Quantum* **2**, 040101 (2021).

[9] D. Gottesman, Fault-Tolerant Quantum Computation with Constant Overhead (2014), [arXiv:1310.2984](https://arxiv.org/abs/1310.2984).

[10] S. Bravyi, A. W. Cross, J. M. Gambetta, D. Maslov, P. Rall, and T. J. Yoder, High-threshold and low-overhead fault-tolerant quantum memory, *Nature* **627**, 778 (2024).

[11] J. R. Wootton and D. Loss, High Threshold Error Correction for the Surface Code, *Phys. Rev. Lett.* **109**, 160503 (2012).

[12] J. Bausch, A. W. Senior, F. J. H. Heras, T. Edlich, A. Davies, M. Newman, C. Jones, K. Satzinger, M. Y. Niu, S. Blackwell, G. Holland, D. Kafri, J. Atalaya, C. Gidney, D. Hassabis, S. Boixo, H. Neven, and P. Kohli, Learning high-accuracy error decoding for quantum processors, *Nature* **635**, 834 (2024).

[13] T. Müller, T. Alexander, M. E. Beverland, M. Bühler, B. R. Johnson, T. Maurer, and D. Vandeth, Improved belief propagation is sufficient for real-time decoding of quantum memory (2025), [arXiv:2506.01779](https://arxiv.org/abs/2506.01779).

[14] H. Cao, F. Pan, Y. Wang, and P. Zhang, qecGPT: Decoding Quantum Error-correcting Codes with Generative Pre-trained Transformers (2023), [arXiv:2307.09025](https://arxiv.org/abs/2307.09025).

[15] Y. Zhao, Y. Ye, H.-L. Huang, Y. Zhang, D. Wu, H. Guan, Q. Zhu, Z. Wei, T. He, S. Cao, F. Chen, T.-H. Chung, H. Deng, D. Fan, M. Gong, C. Guo, S. Guo, L. Han, N. Li, S. Li, Y. Li, F. Liang, J. Lin, H. Qian, H. Rong, H. Su, L. Sun, S. Wang, Y. Wu, Y. Xu, C. Ying, J. Yu, C. Zha, K. Zhang, Y.-H. Huo, C.-Y. Lu, C.-Z. Peng, X. Zhu, and J.-W. Pan, Realization of an Error-Correcting Surface Code with Superconducting Qubits, *Phys. Rev. Lett.* **129**, 030501 (2022).

[16] C. K. Andersen, A. Remm, S. Lazar, S. Krinner, N. Lacroix, G. J. Norris, M. Gabureac, C. Eichler, and A. Wallraff, Repeated quantum error detection in a surface code, *Nat. Phys.* **16**, 875 (2020).

[17] E. Rosenfeld, C. Gidney, G. Roberts, A. Morvan, N. Lacroix, D. Kafri, J. Marshall, M. Li, V. Sivak, D. Abanin, A. Abbas, R. Acharya, L. A. Beni, G. Aigeldinger, R. Alcaraz, S. Alcaraz, T. I. Andersen, M. Ansmann, F. Arute, K. Arya, W. Askew, N. Asstrakhantsev, J. Atalaya, R. Babbush, B. Ballard, J. C. Bardin, H. Bates, A. Bengtsson, M. B. Karimi, A. Bilmes, S. Bilodeau, F. Borjans, J. Bovaird, D. Bowers, L. Brill, P. Brooks, M. Broughton, D. A. Browne, B. Buchea, B. B. Buckley, T. Burger, B. Burkett, N. Bushnell, J. Busnaina, A. Cabrera, J. Campero, H.-S. Chang, S. Chen, Z. Chen, B. Chiaro, L.-Y. Chih, A. Y. Cleland, B. Cochrane, M. Cockrell, J. Cogan, P. Conner, H. Cook, R. G. Cortiñas, W. Courtney, A. L. Crook, B. Curtin, M. Damyanov, S. Das, D. M. Debroy, S. Demura, P. Donohoe, I. Drozdov, A. Dunsworth, V. Ehimhen, A. Eickbusch, A. M. Elbag, L. Ella, M. Elzouka, D. Enriquez, C. Erickson, L. Faoro, V. S. Ferreira, M. Flores, L. F. Burgos, S. Fontes, E. Forati, J. Ford, B. Foxen, M. Fukami, A. W. L. Fung, L. Fuste, S. Ganjam, G. Garcia, C. Garrick, R. Gasca, H. Gehring, R. Geiger, É. Genois, W. Giang, D. Gilboa, J. E. Goeders, E. C. Gonzales, R. Gosula, S. J. de Graaf, A. G. Dau, D. Graumann, J. Grebel, A. Greene, J. A. Gross, J. Guerrero, L. L. Guevel, T. Ha, S. Habegger, T. Hadick, A. Hadjikhani, M. C. Hamilton, M. Hansen, M. P. Harrigan, S. D. Harrington, J. Hartshorn, S. Heslin, P. Heu, O. Higgott, R. Hiltermann, J. Hilton, H.-Y. Huang, M. Hucka, C. Hudspeth, A. Huff, W. J. Huggins, L. B. Ioffe, E. Jeffrey, S. Jevons, Z. Jiang, X. Jin, C. Joshi, P. Juhas, A. Kabel, H. Kang, K. Kang, A. H. Karamlou, R. Kaufman, K. Kechedzhi, T. Khattar, M. Khezri, S. Kim, P. V. Klimov, C. M. Knaut, B. Kobrin, A. N. Korotkov, F. Kostritsa, J. M. Kreikebaum, R. Kudo, B. Kueffler, A. Kumar, V. D. Kurilovich, V. Kutsko, T. Lange-Dei, B. W. Langley, P. Laptev, K.-M. Lau, E. Leavell, J. Ledford, J. Lee, K. Lee, B. J. Lester, W. Leung, L. Li, W. Y. Li, A. T. Lill, W. P. Livingston, M. T. Lloyd, A. Locharla, L. D. Lorenzo, E. Lucero, D. Lundahl, A. Lunt, S. Madhuk, A. Maiti, A. Maloney, S. Mandrà, L. S. Martin, O. Martin, E. Mascot, P. M. Das, D. Maslov, M. Mathews, C. Maxfield, J. R. McClean, M. McEwen, S. Meeks, A. Megrant, K. C. Miao, Z. K. Minev, R. Molavi, S. Molina, S. Montazeri, C. Neill, M. Newman, A. Nguyen, M. Nguyen, C.-H. Ni, M. Y. Niu, N. Noll, L. Oas, W. D. Oliver, R. Orosco, K. Ottosson, A. Pagano, A. D. Paolo, S. Peek, D. Peterson, A. Pizzuto, E. Portoles, R. Potter, O. Pritchard, M. Qian, C. Quintana, G. Ramachandran, A. Ranadive, M. J. Reagor, R. Resnick, D. M. Rhodes, D. Riley, R. Rodriguez, E. Ropes, L. B. D. Rose, E. Rosenberg, D. Rosenstock, E. Rossi, P. Roushan, D. A. Rower, R. Salazar, K. Sankaragomathi, M. C. Sarihan, M. Schaefer, S. Schroeder, H. F. Schurkus, A. Shahingohar, M. J.

Shearn, A. Shorter, N. Shutty, V. Shvarts, S. Small, W. C. Smith, D. A. Sobel, B. Spells, S. Springer, G. Sterling, J. Suchard, A. Szasz, A. Sztein, M. Taylor, J. P. Thiruraman, D. Thor, D. Timucin, E. Tomita, A. Torres, M. M. Torunbalci, H. Tran, A. Vaishnav, J. Vargas, S. Vdovichev, G. Vidal, B. Villalonga, C. V. Heidweiller, M. Voorhees, S. Waltman, J. Waltz, S. X. Wang, D. Wang, B. Ware, J. D. Watson, Y. Wei, T. Weidel, T. White, K. Wong, B. W. K. Woo, C. J. Wood, M. Woodson, C. Xing, Z. J. Yao, P. Yeh, B. Ying, J. Yoo, N. Yosri, E. Young, G. Young, A. Zalcman, R. Zhang, Y. Zhang, N. Zhu, N. Zobrist, Z. Zou, H. Neven, S. Boixo, C. Jones, J. Kelly, A. Bourassa, and K. J. Satzinger, Magic state cultivation on a superconducting quantum processor (2025), [arXiv:2512.13908](https://arxiv.org/abs/2512.13908).

[18] S.-H. Lee, L. English, and S. D. Bartlett, Efficient Post-Selection for General Quantum LDPC Codes (2025), [arXiv:2510.05795](https://arxiv.org/abs/2510.05795).

[19] A. Hutter, J. R. Wootton, and D. Loss, Efficient Markov chain Monte Carlo algorithm for the surface code, *Phys. Rev. A* **89**, 022326 (2014).

[20] H. Bombín, M. Pant, S. Roberts, and K. I. Seetharam, Fault-Tolerant Postselection for Low-Overhead Magic State Preparation, *PRX Quantum* **5**, 010302 (2024).

[21] C. Gidney, M. Newman, P. Brooks, and C. Jones, Yoked surface codes, *Nat. Commun.* **16**, 4498 (2025).

[22] S. C. Smith, B. J. Brown, and S. D. Bartlett, Mitigating errors in logical qubits, *Commun. Phys.* **7**, 386 (2024).

[23] E. Dennis, A. Kitaev, A. Landahl, and J. Preskill, Topological quantum memory, *J. Math. Phys.* **43**, 4452 (2002).

[24] O. Higgott and C. Gidney, Sparse Blossom: Correcting a million errors per core second with minimum-weight matching, *Quantum* **9**, 1600 (2025).

[25] L. Chen, J. Xu, I. Djurdjevic, and S. Lin, Near-shannon-limit quasi-cyclic low-density parity-check codes, *IEEE Transactions on Communications* **52**, 1038 (2004).

[26] P. Panteleev and G. Kalachev, Degenerate Quantum LDPC Codes With Good Finite Length Performance, *Quantum* **5**, 585 (2021).

[27] J. Roffe, D. R. White, S. Burton, and E. Campbell, Decoding across the quantum low-density parity-check code landscape, *Phys. Rev. Res.* **2**, 043423 (2020).

[28] D. Horsman, A. G. Fowler, S. Devitt, and R. V. Meter, Surface code quantum computing by lattice surgery, *New J. Phys.* **14**, 123011 (2012).

[29] X. Tan, F. Zhang, R. Chao, Y. Shi, and J. Chen, Scalable Surface-Code Decoders with Parallelization in Time, *PRX Quantum* **4**, 040344 (2023).

[30] L. Skoric, D. E. Browne, K. M. Barnes, N. I. Gillespie, and E. T. Campbell, Parallel window decoding enables scalable fault tolerant quantum computation, *Nat. Commun.* **14**, 7040 (2023).

[31] A. Gong, S. Cammerer, and J. M. Renes, Toward Low-latency Iterative Decoding of QLDPC Codes Under Circuit-Level Noise (2024), [arXiv:2403.18901](https://arxiv.org/abs/2403.18901).

[32] N. Delfosse and N. H. Nickerson, Almost-linear time decoding algorithm for topological codes, *Quantum* **5**, 595 (2021).

[33] N. Delfosse, V. Londe, and M. E. Beverland, Toward a union-find decoder for quantum ldpc codes, *IEEE Transactions on Information Theory* **68**, 3187 (2022).

[34] T. Hillmann, L. Berent, A. O. Quintavalle, J. Eisert, R. Wille, and J. Roffe, Localized statistics decoding for quantum low-density parity-check codes, *Nat. Commun.* **16**, 8214 (2025).

[35] S. Wolanski and B. Barber, Ambiguity Clustering: An accurate and efficient decoder for qLDPC codes (2025), [arXiv:2406.14527](https://arxiv.org/abs/2406.14527).

[36] J. Chen, Z. Yi, Z. Liang, and X. Wang, Improved Belief Propagation Decoding Algorithms for Surface Codes, *IEEE Transactions on Quantum Engineering* **6**, 1 (2025).

[37] L. A. Beni, O. Higgott, and N. Shutty, Tesseract: A Search-Based Decoder for Quantum Error Correction (2025), [arXiv:2503.10988](https://arxiv.org/abs/2503.10988).

[38] H. Yao, W. A. Laban, C. Häger, A. G. i. Amat, and H. D. Pfister, Belief propagation decoding of quantum ldpc codes with guided decimation, in *2024 IEEE International Symposium on Information Theory (ISIT)* (2024) pp. 2478–2483.

[39] K. R. Ott, B. Hetényi, and M. E. Beverland, Decision-tree decoders for general quantum LDPC codes (2025), [arXiv:2502.16408](https://arxiv.org/abs/2502.16408).

[40] H. Cao, S. Zhao, D. Feng, Z. Shen, H. Yan, T. Su, W. Sun, H. Xu, F. Pan, H. Yu, and P. Zhang, Exact Decoding of Quantum Error-Correcting Codes, *Phys. Rev. Lett.* **134**, 190603 (2025).

[41] M. Wang and F. Mueller, Coprime Bivariate Bicycle Codes and Their Layouts on Cold Atoms (2025), [arXiv:2408.10001](https://arxiv.org/abs/2408.10001).

[42] H. Zhou, C. Zhao, M. Cain, D. Bluvstein, N. Maskara, C. Duckering, H.-Y. Hu, S.-T. Wang, A. Kubica, and M. D. Lukin, Low-Overhead Transversal Fault Tolerance for Universal Quantum Computation, *Nature* **646**, 303 (2025).

[43] D. Litinski, A Game of Surface Codes: Large-Scale Quantum Computing with Lattice Surgery, *Quantum* **3**, 128 (2019).

[44] Y. Li, A magic state's fidelity can be superior to the operations that created it, *New J. Phys.* **17**, 023037 (2015).

[45] D. Litinski, Magic State Distillation: Not as Costly as You Think, *Quantum* **3**, 205 (2019).

[46] C. Gidney, N. Shutty, and C. Jones, Magic state cultivation: Growing T states as cheap as CNOT gates (2024), [arXiv:2409.17595](https://arxiv.org/abs/2409.17595).

[47] Y. Hirano, R. Toshio, T. Itogawa, and K. Fujii, Efficient magic state cultivation with lattice surgery (2025), [arXiv:2510.24615](https://arxiv.org/abs/2510.24615).

[48] H. Yamasaki and M. Koashi, Time-Efficient Constant-Space-Overhead Fault-Tolerant Quantum Computation, *Nat. Phys.* **20**, 247 (2024).

[49] S. Tamiya, M. Koashi, and H. Yamasaki, Polylog-time- and constant-space-overhead fault-tolerant quantum computation with quantum low-density parity-check codes (2024), [arXiv:2411.03683](https://arxiv.org/abs/2411.03683).

[50] Q. T. Nguyen and C. A. Pattison, Quantum fault tolerance with constant-space and logarithmic-time overheads (2024), [arXiv:2411.03632](https://arxiv.org/abs/2411.03632).

[51] G. Zhang, Y. Zhu, X. Yuan, and Y. Li, Constant-Overhead Magic State Injection into qLDPC Codes with Error Independence Guarantees (2025), [arXiv:2505.06981](https://arxiv.org/abs/2505.06981).

[52] H. Xie, N. Yoshioka, K. Tsubouchi, and Y. Li, Noise-Agnostic Unbiased Quantum Error Mitigation for Logical Qubits, *Phys. Rev. Lett.* **136**, 010603 (2026).

[53] H. Xie, Argument-reweighting, <https://github.com/qHaipengXie/Argument-Reweighting>.

[54] C. Gidney, Stim: a fast stabilizer circuit simulator, *Quantum* **5**, 497 (2021).

- [55] S. Maurya, T. Maurer, M. Bühler, D. Vandeth, and M. E. Beverland, FPGA-tailored algorithms for real-time decoding of quantum LDPC codes (2025), [arXiv:2511.21660](https://arxiv.org/abs/2511.21660).
- [56] T. Maurer, M. Bühler, M. Kröner, F. Haverkamp, T. Müller, D. Vandeth, and B. R. Johnson, Real-time decoding of the gross code memory with FPGAs (2025), [arXiv:2510.21600](https://arxiv.org/abs/2510.21600).